

Dynamical Fluctuations of Random Walks in Higher-Order Networks

Leonardo Di Gaetano¹,^{*} Giorgio Carugno², Federico Battiston^{1,*} and Francesco Coghi^{3,†}

¹Department of Network and Data Science, Central European University, 1100 Vienna, Austria

²Department of Mathematics, King's College London, Strand, London WC2R 2LS, United Kingdom

³Nordita, KTH Royal Institute of Technology and Stockholm University,

Hannes Alfvéns väg 12, SEa-106 91 Stockholm, Sweden

 (Received 7 April 2023; revised 4 June 2024; accepted 26 July 2024; published 3 September 2024)

Although higher-order interactions are known to affect the typical state of dynamical processes giving rise to new collective behavior, how they drive the emergence of rare events and fluctuations is still an open problem. We investigate how fluctuations of a dynamical quantity of a random walk exploring a higher-order network arise over time. In the quenched case, where the hypergraph structure is fixed, through large deviation theory we show that the appearance of rare events is hampered in nodes with many higher-order interactions, and promoted elsewhere. Dynamical fluctuations are further boosted in an annealed scenario, where both the diffusion process and higher-order interactions evolve in time. Here, extreme fluctuations generated by optimal higher-order configurations can be predicted in the limit of a saddle-point approximation. Our study lays the groundwork for a wide and general theory of fluctuations and rare events in higher-order networks.

DOI: [10.1103/PhysRevLett.133.107401](https://doi.org/10.1103/PhysRevLett.133.107401)

The appearance of fluctuations in dynamical processes is central in determining the future evolution of many real-world systems [1]. The emergence of rare events may be bolstered or hindered by the hosting complex environment, often conveniently modeled as a complex network [2–4]. Large fluctuations in complex networks have been studied across a variety of processes, including percolation [5–8], spreading [9,10], and transport [11–14]. A stream of research has focused on random walks as a versatile model of diffusion in discrete spaces [15–19] and on their rare event properties [20–22]. Large deviation theory has revealed that low-degree nodes are more susceptible than hubs to the appearance of atypical loads, possibly leading to dynamical phase transitions [23–26].

Despite their success, graphs can only provide a constrained description of real-world systems, as links are inherently limited to model pairwise interactions only [27–29]. Yet, from social [30–33] to biological [34–37] networks, in a wide variety of real-world systems interactions may occur among three or more units at a time. Interestingly, taking into account higher-order interactions has shown to lead to new collective phenomena in a variety

of dynamical processes [38], including diffusion [39,40], contagion [41–43], synchronization [44–48], percolation [49], and evolutionary games [50–52]. While such studies have focused on characterizing dynamical behavior at the typical state, understanding fluctuations and rare events driven by the presence of higher-order interactions is to this day still an open problem.

To this end, in this work we propose a study of fluctuations and rare events on higher-order networks using large-deviation theory tools. We focus on random walks on higher-order networks and on an observable that monitors the time the random walker spends in certain regions of the hypergraph. Our study reveals how fluctuations arise in time for a random walk on a fixed hypergraph structure (*quenched* case), and which higher-order structure is optimal to achieve them (*annealed* case). In the quenched case the density of higher-order interactions regulates fluctuations of occupation times, which are hampered around well-connected nodes and enhanced elsewhere. In the annealed case, where the structure of interactions is not *a priori* fixed, the random walk dynamics select the optimal higher-order structure that maximizes fluctuations and rare events are boosted.

In the following, we present a computationally easy-to-handle hypergraph model to introduce a theory of fluctuations for higher-order networks. Our theory and results are further validated in the Supplemental Material [53] by means of extensive numerical simulations on a wide variety of more complex structures with local heterogeneity and with or without starlike structure, as well as more general dynamics of biased random walks.

^{*}Contact author: battistonf@ceu.edu

[†]Contact author: francesco.coghi@su.se

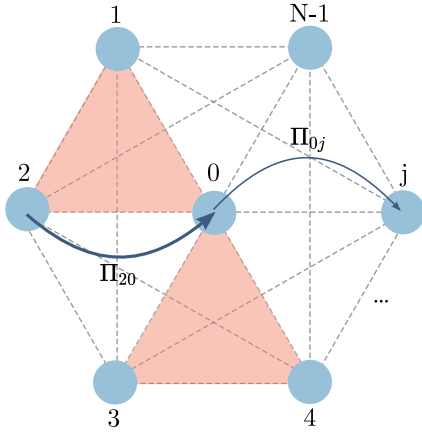


FIG. 1. Illustration of our model. Dashed lines represent pairwise interactions that form the underlying complete graph. In pink, two higher-order interactions connect the core node 0 with the peripheral nodes (1,2), and (3,4). The random walk's dynamics are represented by arrows departing from certain nodes and pointing towards others, where different thicknesses refer to different jump probabilities.

Model—We consider a hypergraph $G = (V, E)$, where V represents the set of nodes, and $E = \{E_1, E_2, \dots, E_M\}$ the set of hyperedges, i.e., E_m is an unordered collection of nodes belonging to the same hyperedge m . We focus in particular on an illustrative structure consisting of a *core* node, labeled 0, connected with *peripheral* nodes through a varying number of higher-order connections, labeled by $i \in \{1, \dots, N-1\}$. As shown in Fig. 1, the graph is composed by $|V| = N$ nodes, a fully connected pairwise structure, i.e., $(N/2)$ binary edges $E_{i(2N-i-1)/2+j} = \{i, j\}$ for $(i, j) \in [0, N-1]^2$ and $i < j$, and a number η drawn from a binomial distribution of parameter $p \in [0, 1]$ of three-body interactions $E_{N(N-1)/2+i} = \{0, i, j\}$, where i is an odd node and $j - i = 1$, i.e., all triangular interactions are centered in 0. We constrain the higher-order structure so that each peripheral node can participate in at most one three-body interaction. As we will show, for this symmetric model, nonpairwise interactions affect the statistics of the core occupation time only through their total number η . In particular, the probability of drawing a hypergraph with a number of three-body interactions $H = \eta$ is given by

$$\mathbb{P}(\eta) := \mathbb{P}(H = \eta) = \binom{N_\Delta}{\eta} p^\eta (1-p)^{N_\Delta - \eta}, \quad (1)$$

where $N_\Delta = \text{ceil}[(N-2)/2]$ is the maximum number of possible three-body interactions that the hypergraph can have.

In summary, G is as an instance of an ensemble of hypergraphs whose higher-order structure is fully described by two parameters only, namely, N and p .

We consider on G an n -step discrete-time random walk $X = \{X_l\}_{l=1}^n$, where X_l denotes the node where the random

walk sits at time l [40]. The random walk follows an unbiased dynamics given by the transition matrix $\Pi = \{\pi_{ij}\}$ whose entries are

$$\pi_{ij} = \frac{k_{ij}^H}{\sum_{l=1}^N k_{il}^H}, \quad (2)$$

where k_{ij}^H represents the hyperdegree, i.e., the number of nodes, excluding i , that are present in the hyperedges that are common to i and j (see Appendix A for details on how to derive the transition matrix). As the random walk explores the graph, it collects information in the form of the time-additive observable

$$T_n = \frac{1}{n} \sum_{l=1}^n \delta_{X_l, 0}, \quad (3)$$

which measures the fraction of time the random walk has spent on the core node 0 up to time n . In the limit of $n \rightarrow \infty$, the typical fraction of time $T_{\eta, \text{typ}}$ the walker spends in 0 for a number $H = \eta$ of three-body interactions reads [40]

$$T_{\eta, \text{typ}} = \frac{4\eta + N - 1}{8\eta + (N - 1)^2}. \quad (4)$$

The higher the number of triangular interactions, the better connected the core with the periphery of the graph, and the longer the time the random walk will spend in 0. Having delineated the typical behavior of the dynamical process, we now focus on its finite-time fluctuations. We consider dynamical fluctuations in two different physical scenarios. First, we study the mean behavior of rare events of T_n over the ensemble of possible hypergraphs of our model (quenched case). Then, at the expense of an entropic cost associated with the logarithm of $P(\eta)$ in (1), we let the random walk choose the optimal hypergraph that generates a particular atypical fluctuation of T_n (annealed case). Results for more complex higher-order topologies, and for more general dynamics considering random walks biased on the higher-order structure, are qualitatively consistent and illustrated in the Supplemental Material [53].

Quenched fluctuations—In the quenched scenario, we consider averaged fluctuations in static hypergraph structures with η three-body interactions and investigate how higher-order network configurations impact the dynamics of random walks. To do so, we employ large deviation theory [54–56], making use of the leading scaling behavior of the probability distribution $\mathbb{P}_{\eta, n}(t) := \mathbb{P}_{\eta, n}(T_n = t)$ that is exponential in time, i.e.,

$$\mathbb{P}_{\eta, n}(t) = e^{-nI_\eta(t) + o(n)}, \quad (5)$$

where $I_\eta(t)$ is the non-negative large-deviation rate function containing the relevant information about rare events

and $o(n)$ denotes sublinear corrections in n . Evaluating I_η directly is often nontrivial, thus we resort to a change of ensemble to get meaningful information on fluctuations. To this end, we introduce the scaled cumulant generating function (SCGF)

$$\Psi_\eta(s) = \lim_{n \rightarrow \infty} \frac{1}{n} \ln G_{\eta,n}(s) = \lim_{n \rightarrow \infty} \frac{1}{n} \ln \mathbb{E}[e^{nsT_n}], \quad (6)$$

which characterizes the leading exponential behavior of the moment generating function $G_{\eta,n}(s)$ associated with T_n . Here, s , the Laplace parameter that enters in the SCGF, plays the role of the conjugate parameter to T_n . Intuitively, as much as the inverse temperature in equilibrium statistical mechanics is connected to the internal energy of a system through the derivative of the canonical free energy, s is connected to the observable T_n . When $s > 0$, T_n will more likely take values that are larger than the typical value and vice versa when $s < 0$. For finite and connected hypergraphs, $\Psi_\eta(s)$ is analytic, and one can calculate $I_\eta(t)$ via the Gärtner–Ellis theorem [54–57] that makes use of the Legendre–Fenchel (LF) transform

$$I_\eta(t) = \sup_{s \in \mathbb{R}} (st - \Psi_\eta(s)), \quad (7)$$

which links the Laplace parameter s with a fluctuation $T_n = t$ as

$$t = \Psi'_\eta(s). \quad (8)$$

Because the random walk X is ergodic, the SCGF can be obtained as

$$\Psi_\eta(s) = \ln \zeta_s, \quad (9)$$

where ζ_s , computed numerically, is the dominant eigenvalue of the so-called tilted matrix

$$\Pi_s = \{(\pi_s)_{ij}\} = \{\pi_{ij} e^{s\delta_{0,j}}\}. \quad (10)$$

To account for average properties of the ensemble of hypergraphs considered, one can take a quenched average over the disorder—here characterized by the number η of higher-order interactions—of the function Ψ_η . Recalling that H is a binomially distributed random variable with parameter p and that the maximum number of higher-order interactions is N_Δ , the quenched average can explicitly be written as

$$\Psi_q(s) = \sum_{\eta=0}^{N_\Delta} \mathbb{P}(\eta) \Psi_\eta(s), \quad (11)$$

where “q” stands for quenched [58]. Given $\Psi_q(s)$ in (11), the quenched rate function $I_q(t)$ can be obtained via an LF transform of Ψ_q (rather than Ψ_η) in (7).

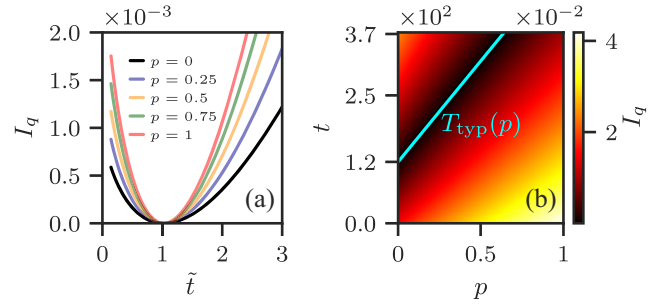


FIG. 2. (a) Rate functions $I_q(\tilde{t})$ as a function of the rescaled time \tilde{t} for different densities of higher-order interactions in the hypergraph p . The higher the p , the narrower the rate functions for $|\tilde{t}| > 1$. (b) Heat map representing how the rate function $I_q(t)$ behaves as a function of t and p (for visualization purposes we plot $\sqrt{I_q}$). The light-blue line represents the typical value T_{typ} which linearly increases with p . Plots obtained for a hypergraph with $N = 1000$ nodes.

To understand the role of higher-order interactions, we first look at whether fluctuations of a given magnitude are more or less likely to appear on higher-order networks generated with different values of p . To understand this, we rescale t in $I_q(t)$ with the typical fraction of time spent in 0 by the random walk at a fixed parameter p , namely, T_{typ} , obtained by averaging (4) over $\mathbb{P}(\eta)$. In Fig. 2(a) we plot the rate functions $I_q(\tilde{t} = t/T_{\text{typ}})$ (\tilde{t} is the time fraction on the core node relative to typical time) for different values of p . Because of the rescaling, all rate functions are 0 at the typical value $\tilde{t} = 1$. The likelihood is encoded in the shape of the rate function branches, the higher (lower) the branch the exponentially less (more) likely is a fluctuation $\tilde{t} \neq 1$ to appear. We notice that with increasing p the average number of higher-order interactions pointing to node 0 grows generating a “confinement” effect, which has two consequences on the dynamics. First, at fixed p , fluctuations are more likely for times greater than the typical time, making it easier to visit the core node than peripheral nodes, as revealed by the asymmetric shape of the rate functions in Fig. 2(a). Moreover, as p increases the transition towards the core node is favored, and fluctuations, both in excess and in deficit relative to the typical time, are hampered, as evidenced by the narrowing of the rate functions with increasing p in Fig. 2(a).

More in detail, in Fig. 2(b) we show how I_q depends both on the nonrescaled time t and p . We observe that the typical time increases with p but also that relative time changes are associated with bigger absolute fluctuations [the level lines of $I_q(p, t)$ are not parallel to T_{typ}]. Moreover, comparing with the case of a fully pairwise graph ($p = 0$), on the one hand we show that the typical behavior at greater p is atypical for the case $p = 0$. On the other hand, rare values of T_n greater than the typical one for the case $p = 0$ can become typical just by increasing the number of higher-order interactions. By contrast, rare values of T_n smaller

than the typical one become even more atypical by introducing higher-order interactions.

Annealed fluctuations—We now consider random walks defined on nonstatic hypergraphs. Such an annealed [59] scenario is relevant to predict dynamical behaviors in time-varying systems where the structure evolves at a rate that is comparable to the timescale of the process on top [60], or in large systems whose precise characterization is often limited by lack of data or noise [61]. In particular, we investigate the annealed fluctuations of the occupation time observable in (3) over nonfixed realizations of three-body interactions for the model introduced above. In such a scenario, large fluctuations of a dynamical observable, such as T_n , could be generated by an optimal, albeit rare, realization of the underlying structure.

We consider the joint probability of obtaining a realization of the higher order structure and the occupation time in (3), and compute the moment generating function $G_n(s)$ associated with the observable T_n with respect to this probability. We notice that $G_n(s)$ takes the form of an *annealed* average of the moment generating function $G_{\eta,n}$ over the disorder

$$G_n(s) = \sum_{\eta=0}^{N_\Delta} \mathbb{P}(\eta) G_{\eta,n}(s), \quad (12)$$

where we remind the reader that fixing s corresponds to fixing a fluctuation t (on average) according to (8).

We consider the regime of long times and large graphs, with the condition $n \gg N_\Delta \gg 1$, and introduce the fraction of total triangles $h = \eta/N_\Delta$. The moment generating function $G_n(s)$ can be expressed using a saddle point approximation in (h, t) , i.e.,

$$G_n(s) \approx e^{n(\ell^{-1} \log \mathbb{P}(h^*) + \Psi_{\eta^*}(s))}, \quad (13)$$

where we call $\ell = n/N_\Delta$ the *annealing parameter* and indicate the saddle-point solution with (h^*, t^*) , adopting the shorthand notation $\eta^* = h^* N_\Delta$. In the following, we focus on the nontrivial exponent of (13):

$$\hat{\Psi}_\ell(s) := \ell^{-1} \log \mathbb{P}(h^*) + \Psi_{\eta^*}(s). \quad (14)$$

We can obtain the annealed SCGF from (14) by taking the infinite ℓ limit, that is $\Psi_a(s) := \hat{\Psi}_{\ell \rightarrow \infty}(s)$. The function $\Psi_a(s)$, together with its LF transform $I_a(t)$, completely describes atypical fluctuations of occupation times in the annealed regime. For large values of ℓ , disorder and dynamics “interact” at the saddle-point solution of (13) selecting the most likely structure that realizes the occupation-time fluctuation associated with s . We remark that (13) is valid as long as ℓ is large [62]. However, since the disorder is self-averaging, in the limit $\ell \rightarrow 0$ all probability concentrates around the typical number of higher-order

interactions, recovering the quenched average (11) for a fixed p .

In Fig. 3(a) we plot \hat{I}_ℓ for several values of ℓ . As expected, for small ℓ we retrieve the quenched rate function I_q (for the parameter $p = 0.5$ used here) which is realized by the typical number of higher-order interactions $\eta^* = h^* N_\Delta \sim \text{ceil}[N_\Delta/2]$ throughout all fluctuations shown in Fig. 3(b). As we increase ℓ , the function \hat{I}_ℓ tends to flatten, and in the limit $\ell \rightarrow \infty$ the annealed rate function I_a develops a plateau of zeros [63]. Although I_a exhibits a continuous range where it equals zero, not every occupation time t within this range is a typical event. Within the saddle-point approximation in (13), it appears that only the times resulting from the most probable network configurations, which manifest at the boundaries of this zero plateau, truly represent the typical behavior of the observable T_n . These specific configurations, as shown in Fig. 3(b), are statistically favored and dominate the ensemble. To further validate our observations, in Fig. 3(a) we also plot Monte Carlo (MC) simulations for both the quenched and annealed case. Details on how to perform such simulations and their physical interpretations are reported in Appendixes B and C. Quenched simulations appear as colored cross-shaped scatter points for three different

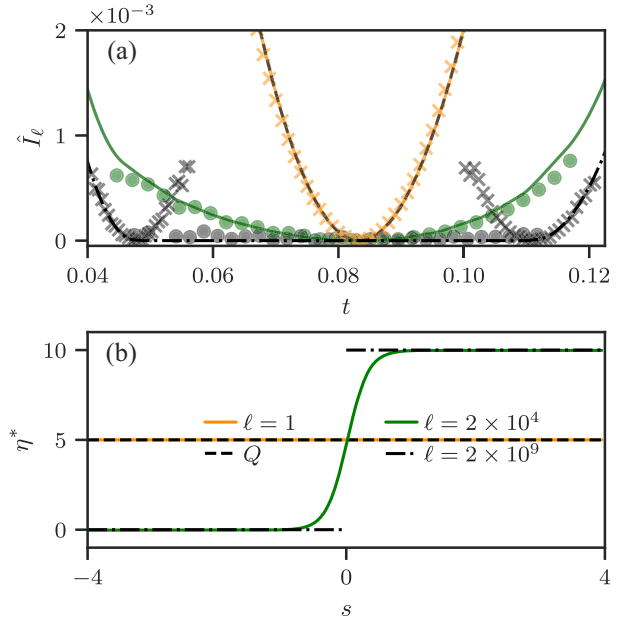


FIG. 3. (a) Rate functions \hat{I}_ℓ functions for different ℓ , as a function of t . Monte Carlo quenched simulations for the three cases with no (leftmost), maximum (rightmost), and half-maximum (center) number of higher-order interactions are plotted as cross-shaped scatter points. Annealed simulation results are plotted as round scatter points for different values of ℓ , colored according to the legend. (b) The optimal value η^* of the number of higher-order interactions plotted as a function of s (the fluctuation parameter). Results are obtained for a hypergraph with $N = 21$ nodes and $p = 0.5$.

scenarios of random walks exploring a graph with no (leftmost gray), max (rightmost gray), and half-max (orange) number of higher-order interactions. Annealed simulations appear as enlarged green and gray scatter points for two different values of ℓ . In particular, orange crosses well describe the shape of the quenched rate function I_q and gray circles well show the flattening of the function \hat{I}_ℓ at large values of ℓ . Noticeably, from the saddle-point calculation in Fig. 3(b) it is evident that for large values of ℓ as one slightly moves from the typical scenario $s = 0$ and looks into fluctuations for either $s < 0$ or $s > 0$, the structure η^* optimally realising such fluctuations abruptly changes from, respectively, a graph with no higher-order interactions, i.e., $\min(\eta^*) = 0$, to a structure that maximizes their number, i.e., $\max(\eta^*) = 10$ for $N = 21$.

For finite ℓ we observe a continuous crossover centered in $s = 0$ between these two regimes. For large ℓ , such crossover appears to be much steeper, hinting at the existence of a transition in the limit $\ell \rightarrow \infty$ between two regimes, one where the random walk spreads over the entire graph, and one where it spends more time on the core node due to higher-order interactions. As discussed in Appendix C and in the Supplemental Material [53], this behavior is an artifact of the saddle-point approximation. Indeed, the existence of a phase transition is not confirmed by an analysis of the distribution of T_n at large ℓ of simulations of random walks on evolving hypergraphs, which converge to an unimodal distribution with $\ell \rightarrow \infty$. This suggests that the observed flattening might be due to neglecting subleading $o(n)$ terms in Eq. (13). Furthermore, the lack of an exponential scaling in the bulk distribution of T_n indicates that typical fluctuations occur more frequently. In summary, while the saddle-point solution is limited in describing fluctuations of the system close to the typical time, it allows to correctly capture the extreme values of the annealed rate function, as confirmed by the good matching between MC simulations and analytical predictions in the tails of the rate functions.

Conclusion—In this work we have shed light on the impact of higher-order interactions on the atypical behaviors of dynamical processes on networks. In particular, we have investigated random walks dynamics in a simplified higher-order model, a fully connected pairwise graph with additional random three-body interactions connecting a core node with peripheral nodes. By applying large deviation tools we have derived the leading exponential scaling of fluctuations for a dynamical observable, here considered to be the mean fraction of time the random walk spends on the system nodes. We characterized the dynamics of the system in two different scenarios, showing that the presence of higher-order interactions greatly affects rare events and atypical dynamics. In the quenched case, where the structure of the system is fixed, higher-order interactions inhibit random walk fluctuations of the occupation time at the core. Conversely, in the Supplemental Material [53], we show that fluctuations of the occupation time on

peripheral nodes are enhanced far off the typical occupation time. In the annealed case, averaging over dynamics on non-fixed structures, the random walk dynamics select the optimal structure that realizes a particular fluctuation. In such a scenario, fluctuations of the occupation time are more likely to appear, and by means of a saddle-point approximation, it is possible to capture dynamical fluctuations far from the typical time. In the Supplemental Material [53], we validated our results on complex structures and showed that homogeneous hypergraphs exhibit a nontrivial density of higher-order interactions boosting fluctuations. Finally, results shown here for random walks extend to broader dynamics, such as for large values of the biasing parameter for biased random walks on hypergraphs, where the bias promotes or hampers the visit of nodes with many higher-order interactions. In the future, it might be interesting to broaden our understanding of the impact of specific higher-order structural features, such as scale-free distribution of higher-order interactions [68], community structure [69], or directed hyperedges [70].

Eventually, our work might be proven useful also to characterize the appearance of rare and catastrophic events in the interconnected structure of higher-order systems, or to control patterns of infections in adoption and rumor diffusion in real-world social networks.

Acknowledgments—L. D. G. acknowledges Paolo D. Piana and Francesco D. Ventura for fruitful discussions. L. D. G. thanks O. Sadekar for valuable assistance.

-
- [1] *Extreme Events in Nature and Society*, edited by S. Albeverio, V. Jentsch, and H. Kantz, The Frontiers Collection (Springer, Berlin Heidelberg, 2006).
 - [2] A. Barrat, M. Barthélemy, and A. Vespignani, *Dynamical Processes on Complex Networks* (Cambridge University Press, Cambridge, England, 2008), pp. 1–347.
 - [3] M. E. J. Newman, *Networks: An Introduction* (Oxford University Press, New York, 2010), pp. 1–784.
 - [4] V. Latora, V. Nicosia, and G. Russo, *Contemporary Physics* (Cambridge University Press, Cambridge, England, 2017), p. 575.
 - [5] G. Bianconi, Fluctuations in percolation of sparse complex networks, *Phys. Rev. E* **96**, 012302 (2017).
 - [6] G. Bianconi, Rare events and discontinuous percolation transitions, *Phys. Rev. E* **97**, 022314 (2018).
 - [7] F. Coghi, J. Morand, and H. Touchette, Large deviations of random walks on random graphs, *Phys. Rev. E* **99**, 022137 (2019).
 - [8] A. Kumar, S. Kulkarni, and M. S. Santhanam, Extreme events in stochastic transport on networks, *Chaos* **30**, 043111 (2020).
 - [9] J. Hindes and I. B. Schwartz, Epidemic extinction and control in heterogeneous networks, *Phys. Rev. Lett.* **117**, 028302 (2016).
 - [10] J. Hindes and I. B. Schwartz, Large order fluctuations, switching, and control in complex networks, *Sci. Rep.* **7**, 1 (2017).

- [11] Y. Z. Chen, Z. G. Huang, and Y. C. Lai, Controlling extreme events on complex networks, *Sci. Rep.* **4**, 6121 (2014).
- [12] Y. Z. Chen, Z. G. Huang, H. F. Zhang, D. Eisenberg, T. P. Seager, and Y. C. Lai, Extreme events in multilayer, interdependent complex networks and control, *Sci. Rep.* **5**, 17277 (2015).
- [13] W. Staffeldt and A. K. Hartmann, Rare-event properties of the Nagel-Schreckenberg model, *Phys. Rev. E* **100**, 062301 (2019).
- [14] K. Gupta and M. S. Santhanam, Extreme events in Nagel-Schreckenberg model of traffic flow on complex networks, *Eur. Phys. J. Special Topics* **230**, 3201 (2021).
- [15] J. D. Noh and H. Rieger, Random walks on complex networks, *Phys. Rev. Lett.* **92**, 118701 (2004).
- [16] M. Rosvall, A. Trusina, P. Minnhagen, and K. Sneppen, Networks and cities: An information perspective, *Phys. Rev. Lett.* **94**, 028701 (2005).
- [17] J. Gómez-Gardeñes and V. Latora, Entropy rate of diffusion processes on complex networks, *Phys. Rev. E* **78**, 065102 (R) (2008).
- [18] Z. Burda, J. Duda, J. M. Luck, and B. Waclaw, Localization of the maximal entropy random walk, *Phys. Rev. Lett.* **102**, 160602 (2009).
- [19] R. Sinatra, J. Gómez-Gardeñes, R. Lambiotte, V. Nicosia, and V. Latora, Maximal-entropy random walks in complex networks with limited information, *Phys. Rev. E* **83**, 030103 (2011).
- [20] V. Kishore, M. S. Santhanam, and R. E. Amritkar, Extreme events on complex networks, *Phys. Rev. Lett.* **106**, 188701 (2011).
- [21] V. Kishore, M. S. Santhanam, and R. E. Amritkar, Extreme events and event size fluctuations in biased random walks on networks, *Phys. Rev. E* **85**, 056120 (2012).
- [22] G. Gandhi and M. S. Santhanam, Biased random walkers and extreme events on the edges of complex networks, *Phys. Rev. E* **105**, 014315 (2022).
- [23] C. De Bacco, A. Guggiola, R. Kühn, and P. Paga, Rare events statistics of random walks on networks: Localisation and other dynamical phase transitions, *J. Phys. A* **49**, 184003 (2016).
- [24] F. Coghi, F. Radicchi, and G. Bianconi, Controlling the uncertain response of real multiplex networks to random damage, *Phys. Rev. E* **98**, 062317 (2018).
- [25] R. Gutierrez and C. Perez-Espigares, Generalized optimal paths and weight distributions revealed through the large deviations of random walks on networks, *Phys. Rev. E* **103**, 022319 (2021).
- [26] G. Carugno, P. Vivo, and F. Coghi, Delocalization-localization dynamical phase transition of random walks on graphs, *Phys. Rev. E* **107**, 024126 (2023).
- [27] F. Battiston, G. Cencetti, I. Iacopini, V. Latora, M. Lucas, A. Patania, J.-G. Young, and G. Petri, Networks beyond pairwise interactions: Structure and dynamics, *Phys. Rep.* **874**, 1 (2020).
- [28] F. Battiston and G. Petri, *Higher-Order Systems* (Springer, New York, 2022).
- [29] C. Berge, *Graphs and Hypergraphs* (North-Holland Pub. Co., Amsterdam, 1973).
- [30] A. Patania, G. Petri, and F. Vaccarino, The shape of collaborations, *EPJ Data Sci.* **6**, 1 (2017).
- [31] A. R. Benson, R. Abebe, M. T. Schaub, A. Jadbabaie, and J. Kleinberg, Simplicial closure and higher-order link prediction, *Proc. Natl. Acad. Sci. U.S.A.* **115**, E11221 (2018).
- [32] G. Cencetti, F. Battiston, B. Lepri, and M. Karsai, Temporal properties of higher-order interactions in social networks, *Sci. Rep.* **11**, 1 (2021).
- [33] F. Musciotto, D. Papageorgiou, F. Battiston, and D. R. Farine, Beyond the dyad: Uncovering higher-order structure within cohesive animal groups, *bioRxiv* (2022).
- [34] S. Klamt, U.-U. Haus, and F. Theis, Hypergraphs and cellular networks, *PLoS Comput. Biol.* **5**, e1000385 (2009).
- [35] G. Petri, P. Expert, F. Turkheimer, R. Carhart-Harris, D. Nutt, P. J. Hellyer, and F. Vaccarino, Homological scaffolds of brain functional networks, *J. R. Soc. Interface* **11**, 20140873 (2014).
- [36] C. Giusti, R. Ghrist, and D. S. Bassett, Two's company, three (or more) is a simplex, *J. Comput. Neurosci.* **41**, 1 (2016).
- [37] A. Zimmer, I. Katzir, E. Dekel, A. E. Mayo, and U. Alon, Prediction of multidimensional drug dose responses based on measurements of drug pairs, *Proc. Natl. Acad. Sci. U.S.A.* **113**, 10442 (2016).
- [38] F. Battiston, E. Amico, A. Barrat, G. Bianconi, G. Ferraz de Arruda, B. Franceschiello, I. Iacopini, S. K'efi, V. Latora, Y. Moreno *et al.*, The physics of higher-order interactions in complex systems, *Nat. Phys.* **17**, 1093 (2021).
- [39] M. T. Schaub, A. R. Benson, P. Horn, G. Lippner, and A. Jadbabaie, Random walks on simplicial complexes and the normalized Hodge 1-Laplacian, *SIAM Rev.* **62**, 353 (2020).
- [40] T. Carletti, F. Battiston, G. Cencetti, and D. Fanelli, Random walks on hypergraphs, *Phys. Rev. E* **101**, 022308 (2020).
- [41] I. Iacopini, G. Petri, A. Barrat, and V. Latora, Simplicial models of social contagion, *Nat. Commun.* **10**, 1 (2019).
- [42] L. Neuh"ausser, A. Mellor, and R. Lambiotte, Multibody interactions and nonlinear consensus dynamics on networked systems, *Phys. Rev. E* **101**, 032310 (2020).
- [43] G. Ferraz de Arruda, G. Petri, P. M. Rodriguez, and Y. Moreno, Multistability, intermittency, and hybrid transitions in social contagion models on hypergraphs, *Nat. Commun.* **14**, 1375 (2023).
- [44] M. Lucas, G. Cencetti, and F. Battiston, Multiorder Laplacian for synchronization in higher-order networks, *Phys. Rev. Res.* **2**, 033410 (2020).
- [45] P. S. Skardal and A. Arenas, Higher order interactions in complex networks of phase oscillators promote abrupt synchronization switching, *Commun. Phys.* **3**, 1 (2020).
- [46] A. P. Mill'an, J. J. Torres, and G. Bianconi, Explosive higher-order Kuramoto dynamics on simplicial complexes, *Phys. Rev. Lett.* **124**, 218301 (2020).
- [47] L. V. Gambuzza, F. Di Patti, L. Gallo, S. Lepri, M. Romance, R. Criado, M. Frasca, V. Latora, and S. Boccaletti, Stability of synchronization in simplicial complexes, *Nat. Commun.* **12**, 1 (2021).
- [48] Y. Zhang, M. Lucas, and F. Battiston, Higher-order interactions shape collective dynamics differently in hypergraphs and simplicial complexes, *Nat. Commun.* **14**, 1605 (2023).

- [49] L. Di Gaetano, F. Battiston, and M. Starnini, Percolation and topological properties of temporal higher-order networks, *Phys. Rev. Lett.* **132**, 037401 (2024).
- [50] U. Alvarez-Rodriguez, F. Battiston, G.F. de Arruda, Y. Moreno, M. Perc, and V. Latora, Evolutionary dynamics of higher-order interactions in social networks, *Nat. Hum. Behav.* **5**, 586 (2021).
- [51] A. Civilini, N. Anbarci, and V. Latora, Evolutionary game model of group choice dilemmas on hypergraphs, *Phys. Rev. Lett.* **127**, 268301 (2021).
- [52] A. Civilini, O. Sadekar, F. Battiston, J. Gómez-Gardeñes, and V. Latora, Explosive cooperation in social dilemmas on higher-order networks, *Phys. Rev. Lett.* **132**, 167401 (2024).
- [53] See Supplemental Material at <http://link.aps.org/supplemental/10.1103/PhysRevLett.133.107401> for further validation of the results presented in the main text, including additional analysis and discussions on simulations involving more complex topologies and alternative, more general classes of dynamical processes.
- [54] F. den Hollander, *Large Deviations* (American Mathematical Society, Providence, 2000).
- [55] H. Touchette, The large deviation approach to statistical mechanics, *Phys. Rep.* **478**, 1 (2009).
- [56] A. Dembo and O. Zeitouni, *Large Deviations Techniques and Applications*, Stochastic Modelling and Applied Probability Vol. 38 (Springer, Berlin Heidelberg, 2010).
- [57] R. S. Ellis, *Entropy, Large Deviations, and Statistical Mechanics*, Classics in Mathematics (Springer, New York, 1985).
- [58] Remarkably, the quenched average (11) takes such a simplified form because for a fixed number η of higher-order interactions, we have only one possible transition matrix. However, we note that more complicated models might lead to different disorder configurations and therefore different transition matrices. In the latter case, to disentangle disorder and dynamics one would need to carefully study combinatorially how many different configurations arise by fixing η .
- [59] S. N. Dorogovtsev, A. V. Goltsev, and J. F. F. Mendes, Critical phenomena in complex networks, *Rev. Mod. Phys.* **80**, 1275 (2008).
- [60] B. Guerra and J. Gómez-Gardeñes, Annealed and mean-field formulations of disease dynamics on static and adaptive networks, *Phys. Rev. E* **82**, 035101(R) (2010).
- [61] A. F. Peralta, A. Carro, M. S. Miguel, and R. Toral, Stochastic pair approximation treatment of the noisy voter model, *New J. Phys.* **20**, 103045 (2018).
- [62] In particular, for ℓ finite and small, one has $N_\Delta > n$ and therefore the ergodicity assumption necessary to derive $\Psi_{\eta^*}(s)$ falls.
- [63] That an annealed rate function is a lower bound of a quenched one is known in the mathematics literature [64–67]. Intuitively, this is consequence of picking an optimal structure to generate fluctuations in the dynamics rather than having it fixed as in the quenched case.
- [64] A. Greven and F. den Hollander, Large deviations for a random walk in random environment, *Ann. Probab.* **22**, 1381 (1994).
- [65] F. Comets, N. Gantert, and O. Zeitouni, Quenched, annealed and functional large deviations for one-dimensional random walk in random environment, *Probab. Theory Relat. Fields* **118**, 65 (2000).
- [66] S. R. Varadhan, Large deviations for random walks in a random environment, *Commun. Pure Appl. Math.* **56**, 1222 (2003).
- [67] O. Zeitouni, Random walks in random environments, *J. Phys. A* **39**, R433 (2006).
- [68] K. Kovalenko, I. Sendina-Nadal, N. Khalil, A. Dainiak, D. Musatov, A. M. Raigorodskii, K. Alfaro-Bittner, B. Barzel, and S. Boccaletti, Growing scale-free simplices, *Commun. Phys.* **4**, 43 (2021).
- [69] M. Contisciani, F. Battiston, and C. De Bacco, Inference of hyperedges and overlapping communities in hypergraphs, *Nat. Commun.* **13**, 7229 (2022).
- [70] G. Gallo, G. Longo, S. Pallottino, and S. Nguyen, Directed hypergraphs and applications, *Discrete Appl. Math.* **42**, 177 (1993).

End Matter

Appendix A: Transition matrix of random walk on hypergraphs—In the random walk on hypergraph the walker chooses with equal probability among its hyperlinks and then selects one of the nodes belonging to such a higher-order structure, favoring intrinsically those neighbors that belong to highest-order hyperlinks. In order to write the transition matrix, we start defining the hyper incidence matrix $e_{i\alpha}$ telling if a node i belong to a hyperlink E_α , namely,

$$e_{i\alpha} = \begin{cases} 1 & \text{if } i \in E_\alpha \\ 0 & \text{otherwise} \end{cases}. \quad (\text{A1})$$

From the hyperincidence matrix one can define the hyperadjacency matrix as follows:

$$A = ee^T, \quad (\text{A2})$$

where A_{ij} represents the number of hyperlinks containing both nodes i and j . Furthermore, one can build the hyperedges matrix, $C_{\alpha\beta}$,

$$C = e^T e, \quad (\text{A3})$$

whose entry $C_{\alpha\beta}$ counts the number of common nodes between E_α and E_β ($E_\alpha \cap E_\beta$) and $C_{\alpha\alpha}$ is the size of an hyperlink E_α , or, equivalently, its order of interaction plus one, $|E_\alpha| = O_\alpha + 1$.

By means of C and e , we can construct the weight of the transition matrix of the unbiased random walk, k_{ij}^H , that reads,

$$k_{ij}^H = \sum_{\alpha} (C_{\alpha\alpha} - 1) e_{i\alpha} e_{j\alpha} = (e \hat{C} e^T)_{ij} - A_{ij}, \quad (\text{A4})$$

where its entries represent the sum of the orders of all the common hyperlinks between i and j . Summing k_{ij}^H over all

neighbors of a node i , one obtains the order-weighted hyperdegree,

$$k_i^H = \sum_l k_{il}^H, \quad (\text{A5})$$

namely, the sum of the orders of all the hyperlinks belonging to i .

Therefore, the transition matrix of the unbiased random walk on a hypergraph reads

$$\Pi_{ij} = \frac{\sum_\alpha (C_{\alpha\alpha} - 1) e_{i\alpha} e_{j\alpha}}{\sum_l \sum_\alpha (C_{\alpha\alpha} - 1) e_{i\alpha} e_{l\alpha}} = \frac{k_{ij}^H}{\sum_l k_{il}^H} = \frac{k_{ij}^H}{k_i^H}. \quad (\text{A6})$$

Appendix B: Quenched Monte Carlo simulations—Given a hypergraph of size N with a configuration of higher-order interactions η sampled from the binomial distribution in Eq. (1), we run simulations of length n . The result of this is a histogram of values for the observable T_n for a given hypergraph. We then calculate the rate function [see Eq. (7)] for the observable T_n as

$$I_\eta^{\text{sim}}(t) = -\frac{1}{n} \ln \mathbb{P}_\eta^{\text{hist}}(t), \quad (\text{B1})$$

where superscript “sim” indicates that the function is obtained from simulations and “hist” refers to the fact that the distribution is approximated by the histogram related to the simulations. We repeat the procedure for many configurations of the hypergraph randomly selected from the binomial distribution in Eq. (1) and calculate the rate functions by averaging as follows:

$$I_q^{\text{sim}}(t) = \sum_{\eta=0}^{N_\Delta} \mathbb{P}^{\text{hist}}(\eta) I_\eta^{\text{sim}}(t), \quad (\text{B2})$$

where $\mathbb{P}^{\text{hist}}(\eta)$ is the probability distribution of configurations η at a fixed p obtained with the random generation of graphs [it converges to Eq. (1)]. Notice that the cumulative statistics over different hypergraphs come only after rescaling with $1/n \ln$ each distribution of T_n . These are the quenched simulations represented as gray ($p = 0$ and $p = 1$) and orange ($p = 0.5$) circular dots in Fig. 3(a). They are used as a sanity check both for the quenched limit of our annealed calculation for $p = 0.5$ in the middle and, in the case of the annealed rate function, to check that the extrema of the zeros plateau corresponds to the two opposite situations of a graph with no triangular interactions for $p = 0$ (on the left) and a graph with N_Δ (the maximum possible) triangular interactions for $p = 1$ (on the right).

Appendix C: Annealed Monte Carlo simulations—In order to carefully calculate the Legendre transform of Eq. (14), which is the asymptotic leading behavior of Eq. (12), and visualize the rate functions appearing in Fig. 3(a) we generate many trajectories of the random walk of length n (which in turn fixes the parameter $\ell = n/N_\Delta$ for a graph of N nodes) where each one is initialized over a hypergraph with a number of triangular interactions picked up at random from the binomial distribution in Eq. (1). The graph is resampled over the trajectory of the random walk at a fast rate. Once all the trajectories are obtained we calculate the cumulative statistic (the histogram) of the observable T_n and, only after that, rescale the properly normalized histogram by $1/n \ln$. It is important to stress here that in the annealed scenario the rescaling comes after obtaining the full statistics over all hypergraphs for the observable T_n (notice that this procedure is inverted in the quenched scenario), which is the reason why at the saddle point of Eq. (13) dynamics and disorder “interact.” This procedure already generates a distribution $\mathbb{P}_a^{\text{hist}}$ for the observable T_n and from it we directly calculate the rate function

$$I_a^{\text{sim}}(t) = -\frac{1}{n} \ln \mathbb{P}_a^{\text{hist}}(t). \quad (\text{B3})$$

This is the procedure followed to obtain the annealed simulations plotted in Fig. 3(a).

The histograms of $\mathbb{P}_a^{\text{hist}}$ for different values of n reveal that there is no observable flattening across the simulations. Instead, as n increases, the histograms converge, indicating no true phase transition in the system, see Fig. 4. This suggests that the flattening of the rate function observed in the annealed scenario is caused by solely examining the saddle point in the study of dynamics using large deviations, neglecting subleading contributions.

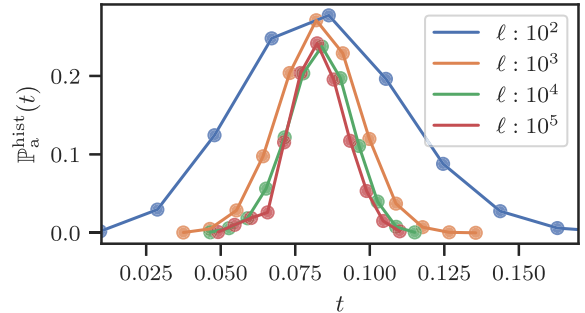


FIG. 4. Histograms of observable T_n from annealed simulations at different values of n ($\ell = n$). The simulations are performed considering $N = 21$, and 10^5 different trajectories.